Inner Macular Changes in Fellow Eye of Patients With Unilateral Idiopathic Epiretinal Membrane

Andrea M. Coppe,[1] Giuliana Lapucci,[2] Guido Ripandelli,[3] Francesca R. Pesci,[3] Luca Buzzonetti,[1] and Giancarlo Iarossi[1]

[1]Bambino Gesù Children's Hospital – IRCCS, Rome, Italy
[2]Studio Oculistico Coppé, Rome, Italy
[3]Fondazione G. B. Bietti per l'Oftalmologia – IRCCS, Rome, Italy

Correspondence: Andrea M. Coppe, Bambino Gesù Children's Hospital – IRCCS, Via della torre di Palidoro, snc, 00050 Fiumicino (Rome), Italy; coppe@fastwebnet.it.

The work was completed in the Fondazione G. B. Bietti per l'Oftalmologia I.R.C.C.S.

Received: March 28, 2021
Accepted: August 5, 2021
Published: August 24, 2021

Citation: Coppe AM, Lapucci G, Ripandelli G, Pesci FR, Buzzonetti L, Iarossi G. Inner macular changes in fellow eye of patients with unilateral idiopathic epiretinal membrane. *Invest Ophthalmol Vis Sci.* 2021;62(10):29. https://doi.org/10.1167/iovs.62.10.29

Purpose. We evaluated a series of fellow eyes (FEs) in patients affected by unilateral idiopathic epiretinal membrane (IERM) with spectral-domain optical coherence tomography (SD-OCT) and OCT angiography (OCT-A) to determine if a previous defect in the inner retina is present before the mechanical damage to the inner limiting membrane (ILM) caused by posterior vitreous detachment.

Methods. In patients with IERM ($N = 39$), ganglion cell layer (GCL) thickness in FEs was assessed with SD-OCT; in a subgroup ($N = 25$) the vessel density (VD) at the superficial (SCP) and deep capillary plexus (DCP) was assessed with swept-source OCT-A (SS-OCT-A). These values were then compared with 30 age-matched healthy control eyes (CEs). The statistical analyses used SPSS software version 15.0 (SPSS, Inc., Chicago, IL, USA). Data collected underwent 1-way ANOVA. A level of $P < 0.05$ was accepted as statistically significant.

Results. The GCL thickness in the FEs was significantly lower than in CEs, with a significant thinning in all sectors except temporal ones (mean $P < 0.001$, superior $P = 0.0002$, superonasal $P < 0.001$, inferonasal $P < 0.001$, and inferior $P = 0.002$). The VD was significantly lower in the FEs in all sectors of SCP (mean $P = 0.009$, inner ring $P = 0.028$, and outer ring $P = 0.007$).

Conclusions. GCL and SCP are significantly reduced in the FEs. These data suggest that a vascular defect in the SCP could cause a cellular loss in the inner retina that may determine the cascade events leading to the IERM proliferation; the diagnosis in a preclinical phase could provide a treatment strategy to prevent the progression of the disease.

Keywords: idiopathic epiretinal membrane (IERM), spectral domain optical coherence tomography (SS-OCT), optical coherence tomography angiography (OCT-A), macular vessel density, macular plexus, ganglion cells, astrocytes, fellow eye (FE)

Epiretinal membranes (ERMs) are characterized by non-vascularized fibrocellular tissue, developing on the vitreoretinal interface and inducing a tangential traction on the macular area. Depending on their etiology, the ERMs are made of glial cells, retinal pigment epithelial (RPE) cells, macrophages, fibrocytes, and collagen, in different proportions.[1]

Idiopathic ERMs (IERMs) are the most common types of ERMs and occur without association with ocular diseases, such as retinal detachment, retinal vein occlusions, and diabetic retinopathy,[2] and previous cataract surgery.

The hypothesis that predisposing conditions for IERMs are present in both eyes of patients is supported by the fact that a prevalence of bilateral IERM of about 30% has been observed.[3,4]

The development of the IERM after posterior vitreous detachment, could be induced by growth factors and cytokines that would elicit the glial cells migration (e.g. Müller cells and astrocytes) into the vitreous through small focal defects at the level of the internal limiting membrane (ILM).[5,6] The proliferation of these cells, or the existing ILM, could be a scaffold for other cell type migration, such as hyalocytes and macrophages, on the vitreoretinal interface.[7,8]

A previous study of Ramirez has described an increased frequency of IERMs in age-related macular degeneration (AMD) eyes and a progressive reduction of number of astrocytes in the retinal ganglion cell layer (GCL) with aging.[9] Astrocytes, like Müller cells, are connected to retinal blood vessels and neurons and play a critical role in providing energy substrates to neurons and regulating the production of trophic factors and antioxidants.[10] Vascular changes that occur in aged patients, together with the loss of astroglial cells, could cause a progressive degeneration of ganglion cells.

Currently, spectral domain optical coherence tomography (SD-OCT) imaging plays a key role in the diagnosis and classification of vitreomacular interface diseases[11] allowing for the observation of preclinical changes. Optical coherence tomography angiography (OCT-A) is a noninvasive,

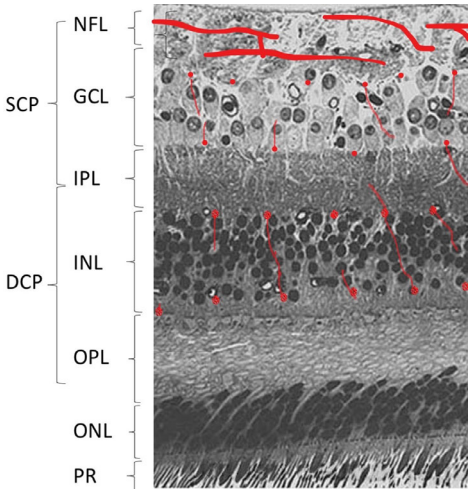

Figure 1. Histological images with overlayed localization of superficial and deep capillary plexus (hand drawn in *red*) in the human retina. NFL, nerve fiber layer; GCL, ganglion cell layer; IPL, inner plexiform layer; INL, inner nuclear layer; OPL, outer plexiform layer; ONL, outer nuclear layer; PR, photoreceptors; RPE, retinal pigmented epithelium.

dye-less imaging technique. It is clinically useful for studying foveal microvascular changes in different retinal vascular diseases[12–16] and in uveitis[17] providing high-resolution scans of retinal and choroidal vasculature detecting erythrocyte movement in blood vessels[18] and allowing for the visualization of the superficial capillary plexus (SCP) and deep capillary plexus (DCP). The SCP is composed of larger arteries, arterioles, capillaries, venules, and veins vessels located primarily in the GCL, whereas the DCP is composed of thinner arterioles, capillaries, venules, and veins vessels located in the inner plexiform, inner nuclear, and outer plexiform layers[19] (Fig. 1).

The aim of this study was to analyze and quantify the thickness of GCL and the vessel density (VD) in the SCP and DCP in the fellow eyes (FEs) of patients with unilateral IERM versus a healthy age-matched control group.

Materials and Methods

All procedures in this study adhered to the tenets of the Declaration of Helsinki and were approved by the investigational review board of Central Ethic Committee IRCCS Lazio. All subjects gave their informed consent after the aim of the study had been fully explained.

Thirty-nine FEs of 39 consecutive patients (17 men and 22 women; mean age = 71.18 ± 10.91 years) with unilateral IERM were enrolled. Thirty eyes of 30 age- and sex-matched healthy subjects with no ocular disease were recruited as controls (14 men and 16 women; mean age = 68.33 ± 12.45 years, $P = 0.315$ vs. FEs group). Only one eye randomly selected was enrolled for inclusion in the control group. Before imaging, all patients underwent ophthalmic examination, including best-corrected visual acuity and fundus examination, performed by a retina specialist using a 90 diopter (D) indirect lens. Inclusion criteria were the presence of IERM in only one eye, associated with absence of any alteration detectable with SD-OCT in the FE. Exclusion criteria were the presence of any retinal or choroidal disease, such as retinal detachment, retino-vascular disease, AMD, diabetic retinopathy, glaucoma or ocular hypertension, a history of ocular laser or surgery, eyes with refractive errors >±3 D, media opacities that prevented good visualization of the fundus, any associated systematic disorders (e.g. systemic corticosteroids intake, diabetes, or hypertension), or vascular diseases without retinopathy, which would affect the VD independent of a FE ERM. SD-OCT imaging exclusion criteria for unaffected FEs were: no changes of the normal foveal profile, flat surface of the analyzed area, and no changes in all the macular layers, including RPE. Mean demographic data and clinical characteristics of patient and CEs are shown in Table 1.

The macula in both FEs and CEs groups was assessed using the SD-OCT (Cirrus 5000; Carl Zeiss Meditec, Inc., Dublin, CA, USA). The device performed each acquisition at a speed of 100 kHz, 68.000 A-scans per second, using an 840-nm superluminescent diode; the macula was analyzed by SD-OCT using the 512 × 128 scan pattern in which a 6 × 6 mm area centered on the fixation point is scanned with 128 B-scan composed by 512 A-scan. The software (version 6.5.0.772) computed the mean macular thickness in the 6 × 6 mm area using a whole Early Treatment Diabetic Retinopathy Study (ETDRS) grid centered on the fixation point, which contains 3 concentric rings of diameters 1, 3, and 6 mm, and 2 reticules to divide the macula into 9 subfields, in each the retinal thickness is separately measured (central: C1; inner ring: S3, N3, I3, and T3 [parafovea]; outer ring: S6, N6, I6, and T6 [perifovea][20]; Fig. 2A).

Using the same 6 × 6 cube scan, the algorithm performed the segmentation of mean thickness of the whole perifoveal GCL, within a 14.13 mm^2 elliptical annulus area (dimensions: a vertical inner and outer diameter of 0.5 and 2.0mm and a horizontal inner and outer diameter of 0.6 and 2.4 mm, respectively) centered on the fovea (Fig. 2B). The size of the inner ring in the annulus was chosen to exclude the foveal area, where the GCL is too thin to be detected; the size and shape of the outer ring was selected because it conforms closely to the real anatomy of the normal retinal ganglion cells distribution in the macular region.

Table 1. Demographic Data and Clinical Characteristics of Patient and Control Eyes

	Control Group ($N = 30$)	Study Group ($N = 39$)	*P* Value
Sex			
M	14	17	–
F	16	22	–
Age (years)	71.18 ± 10.91	68.33 ± 12.45	0.315
IOP (mm Hg)	15.7 ± 1.9	15.3 ± 3.1	0.536
Best corrected visual acuity (LogMAR)	0.041 ± 0.035	0.056 ± 0.042	0.106

Data are reported as mean ± standard deviation; statistical difference between the two groups is also shown for comparison.

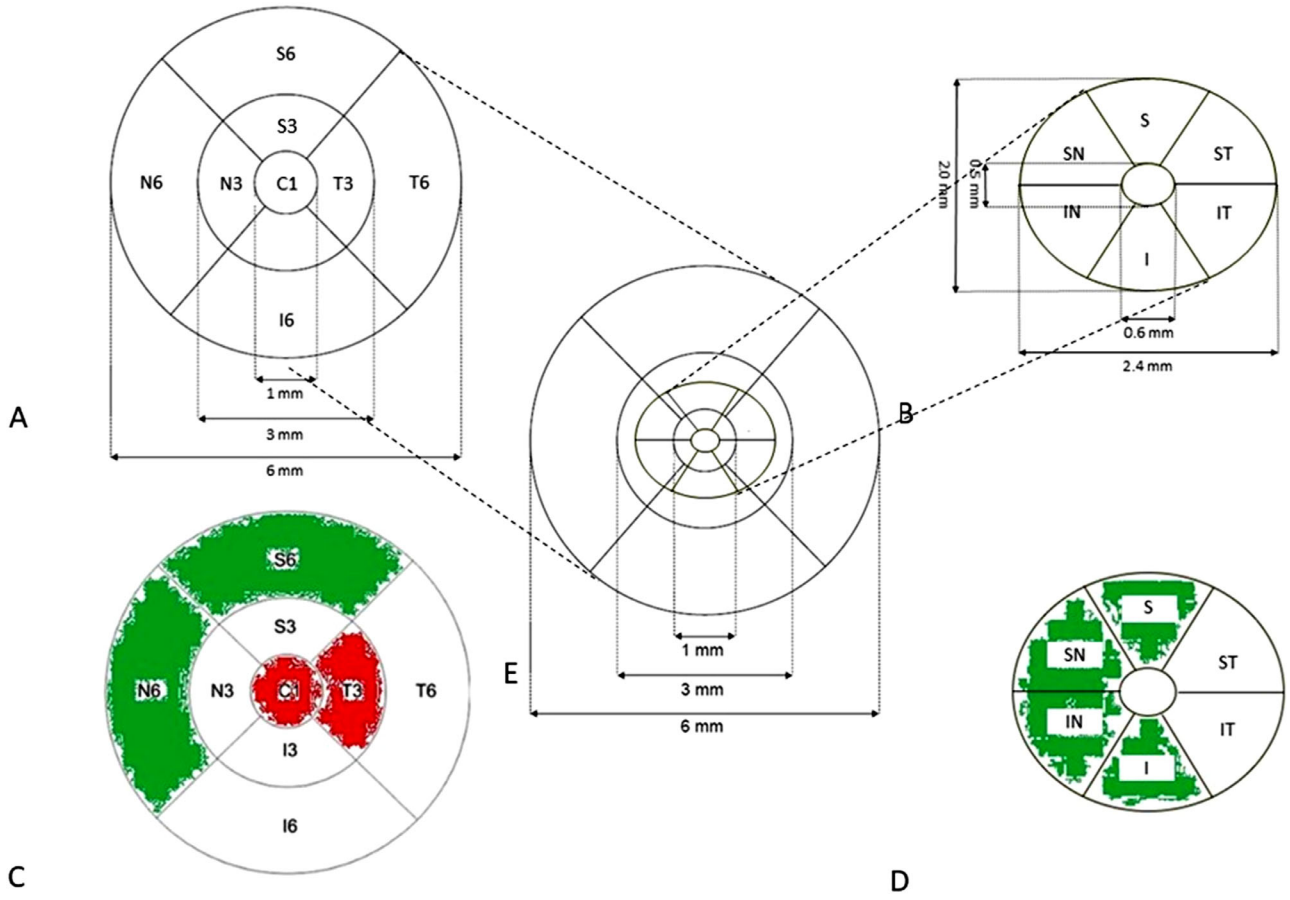

Figure 2. (**A**) ETDRS grid centered on the fixation point containing 3 concentric rings with 1, 3, and 6 mm diameters, divided by 2 reticules into 9 subfields: central (C1); inner superior ring (S3), temporal (T3), inferior (I3) and nasal (N3); outer superior ring (S6), temporal (T6), inferior (I6), and nasal (N6). (**B**) Ganglion cell layer grid (GCL): 14.13mm^2 elliptical annulus area (dimensions: a vertical inner and outer radius of 0.5 and 2.0 mm and a horizontal inner and outer radius of 0.6 and 2.4 mm, respectively) centered on the fovea. Sectors: superior (S); superonasal (SN); inferonasal (IN); inferior (I); inferotemporal (IT); and superotemporal (ST). (**C**) Comparison of retinal thickness between FEs and CEs in each subfield. If the subfield is thicker in FEs as compared to CEs, it is displayed in *red*, if thinner in *green*. If the difference is not statistically significant, it is displayed in *white*. (**D**) Comparison of GCL thickness between FEs and CEs in each subfield. If the subfield is thicker in FEs as compared to CEs, it is displayed in *red*, if thinner in *green*. If the difference is not statistically significant, it is displayed in *white*. (**E**) Overlayed representation of ETDRS and GCL grid.

The algorithm identifies the outer boundary of the nerve fiber layer (NFL) and the outer boundary of the inner plexiform layer (IPL), so that the difference between the NFL and the IPL outer boundary segmentations yields the GCL.[21] The following GCL thickness measurements were analyzed: mean and sectorial: superior (S); superonasal (SN); inferonasal (IN); inferior (I); inferotemporal (IT); and superotemporal (ST; see Fig. 2B).

Images with visible eye motion or blinking artefacts and with poor image quality were excluded (defined as signal strength lower than 5/10).

In a subgroup of 25 patients (14 women and 11 men), and 25 controls (13 women and 12 men), the macula was assessed using the split-spectrum amplitude-decorrelation angiography with PLEX Elite 9000 (version 1.5.0.15909; Carl Zeiss Meditec Inc.). It is a swept-source OCT angiography (SS-OCT-A) that provides automated segmented enface OCT of different plexus: SCP, DCP, avascular retina, choriocapillaris (CC), and choroid (Ch). OCT-A on the PLEX Elite 9000 is generated with the OMAG algorithm (optical microangiography),[22,23] which utilizes the complete complex OCT data signal, including both amplitude and phase, to detect motion of red blood cells within sequential OCT B-scans performed repeatedly at the same location.[23–25] The device performed each acquisition at a speed of 100,000 A-scans per second, using as optical source a swept source tunable laser, center wavelength between 1040 and 1060 nm; axial resolution 6.3 µm, and transverse resolution 20 µm. A 6 × 6 mm cube scan was performed, 500 A-scan made up a B-scan, 500 horizontal B-scan were sampled in the scanning area to form a 6 × 6 mm 3-dimensional data cube.

Images with visible eye motion or blinking artifacts and with poor image quality were excluded (defined as signal strength lower than 7/10). OCTs were visually assessed by the same retina specialist (author A.M.C.) to ensure proper segmentation of the GCL and the SCP and DCP.

The software, using an algorithm that is a prototype provided by the manufacturer (ARI Network - Zeiss), computed the VD in the 6 × 6 mm area using the ETDRS grid centered on the fixation point, which contains 3 concentric rings of diameters 1, 3, and 6 mm, and 2 reticules to

Table 2. Retinal Thickness at the ETDRS Grid in 6 × 6 mm Scan of the Fellow (FEs) and Control (CEs) Eyes

Retinal Thickness (μm)	Mean	S3	N3	I3	T3	S6	N6	I6	T6	C1
FEs $N = 39$	296.47 ± 11.6	327.10 ± 14.7	329.83 ± 15.5	325.50 ± 14.3	318.35 ± 14.0*	275.28 ± 11.1*	294.05 ± 12.3*	266.90 ± 12.4	264.13 ± 11.2	267.08 ± 18.4*
CEs $N = 30$	294.02 ± 12.8	323.60 ± 17.0	326.47 ± 13.8	319.60 ± 17.3	307.00 ± 24.4	280.57 ± 12.2	300.73 ± 13.0	267.77 ± 12.8	260.10 ± 14.4	258.70 ± 19.5
P value	0.527	0.367	0.314	0.159	0.013	0.015	0.014	0.505	0.438	0.033

*$P < 0.05$.

Data are expressed in micron, reported as mean ± standard deviation; thickness values are reported for the specific analyzed areas: mean, inner ring superior (S3), temporal (T3), inferior (I3) and nasal (N3); outer ring superior (S6), temporal (T6), inferior (I6) and nasal (N6); and central (C1). Statistical analysis between the two groups is also reported. Mean macular thickness is slightly increased in FEs as compared to CEs, but the difference is not statistically significant. Subfield analysis shows a retinal thickness significantly higher in the FEs in the central area (C1) and temporal inner ring (T3), lower in nasal outer ring (N6) and superior outer ring (S6). No statistically significant differences were found in the other subfield.

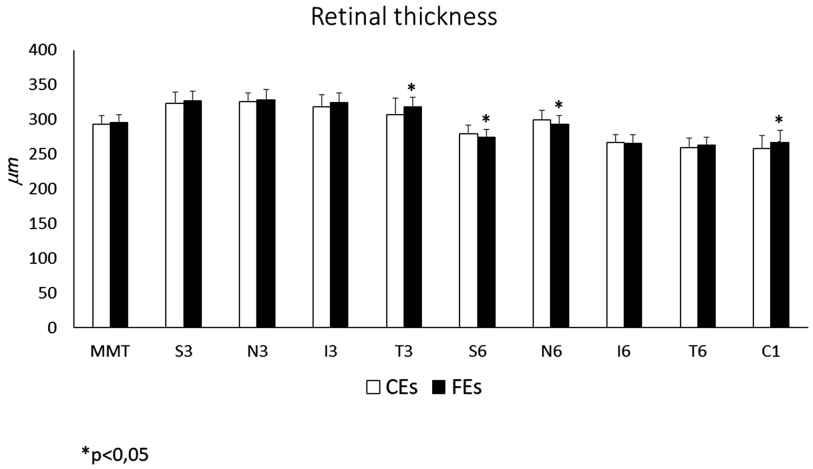

Figure 3. Histograms showing the whole retinal thickness, expressed in micron, (according to the 6 mm ETDRS sectors, see Fig. 2A), of FEs and CEs. Mean macular thickness (MMT) in FEs is slightly, but not significantly, increased as compared to CEs. Subfield analysis shows in FEs a significant thickening in the central area (C1) and temporal inner ring (T3) and a thinning in nasal outer (N6) and superior outer rings (S6). No statistically significant differences are found in the other subfields. Data are presented as mean ± SD, FEs $n = 39$, and CEs $n = 30$. 1-way ANOVA, *$P < 0.05$.

divide the macula into 9 subfields, analogous to the previous described ETDRS grid (central = C1; inner ring = S3, N3, I3, and T3; and outer ring = S6, N6, I6, and T6). As the elliptical annulus area in which the thickness of GCL is computed is not homologous to the ETDRS grid, we chose to compare the VD of more than one perfusion area in FEs and CEs, according to the concept that the analyzed area had to overlap with the elliptical annulus area; therefore, the areas studied were: inner ring (sectors S3, N3, I3, and T3), outer ring (sectors S6, N6, I6, and T6), and 6 mm mean (sectors C1, S3, N3, I3, T3, S6, N6, I6, and T6; see Fig. 2A). Data are expressed as percentage VD.

The statistical analyses used SPSS software version 15.0 (SPSS, Inc., Chicago, IL, USA). The data obtained were analyzed with frequency and descriptive statistics. Data collected underwent 1-way ANOVA. A level of $P < 0.05$ was accepted as statistically significant.

Results

Mean macular thickness was slightly increased in FEs as compared to CEs (296.47 ± 11.68 μm in FEs vs. 294.02 ± 12.81 μm in CEs) but the difference was not statistically significant. However, subfield analysis showed that retinal thickness was significantly higher in the FEs as compared to CEs in the central area (C1 = 267.08 ± 18.49 μm in FEs vs. 258.70 ± 19.52 μm in CEs, $P = 0.033$) and temporal inner ring (T3 = 318.35 ± 14.03 μm in FEs vs. 307.00 ± 24.44 μm in CEs, $P = 0.013$) and significantly lower in nasal outer ring (N6 = 294.05 ± 12.34 μm in FEs vs. 300.73 ± 13.04 μm in CEs, $P = 0.014$) and superior outer ring (S6 = 275.28 ± 11.10 μm in FEs vs. 280.57 ± 12.22 μm in CEs, $P = 0.015$). No statistically significant differences were found in the other subfields. Data are reported in Table 2 and in Figure 3, subfield thickness in FEs are displayed in red if thicker, and in green if thinner in Figure 2C.

Mean GCL thickness in the FEs was significantly lower than in CEs (77.82 ± 6.18 vs. 81.94 ± 4.14, $P = 0.0001$). The subfields analysis showed a significant thinning of CGL in all sectors except temporal ones: (S = 72.79 ± 6.77 in FEs vs. 82.59 ± 4.47 in CEs, $P = 0.0002$; SN = 77.74 ± 6.95 in FEs vs. 83.59 ± 4.99 in CEs, $P < 0.001$; IN = 76.28 ± 7.16 in FEs vs. 81.59 ± 5.14 in CEs, $P < 0.001$; I = 76.46 ± 6.89 in FEs vs. 80.46 ± 4.86 in CEs, $P = 0.002$). GCL thickness data are reported in Table 3 and in Figure 4, the thinner subfields in FEs group are displayed in green in Figure 2D.

The 6 mm mean VD in SCP of FEs was significantly lower than in CEs (0.377 ± 0.076 vs. 0.426 ± 0.048, $P = 0.009$). The subfields analysis showed a statistically significant reduction of VD in FEs versus CEs in all sectors (inner ring = 0.364 ± 0.102 vs. 0.418 ± 0.064, $P = 0.028$; outer ring = 0.388 ± 0.068 vs. 0.434 ± 0.043, $P = 0.007$; Table 4, Fig. 5).

The 6 mm mean VD in DCP of FEs was reduced, but not significantly, as compared to CEs (0.210 ± 0.065 vs. 0.233 ± 0.055, $P = 0.173$). The subfields analysis also showed a reduction, but not statistically significant in all sectors (inner

Table 3. Ganglion Cell Layer Thickness (Mean ± SD) in 6 × 6 mm Scan of the Fellow (FEs) and Control (CEs) Eyes

GCL Thickness (µm)	Mean	ST	S	SN	IN	I	IT
FEs $N = 39$	77.82 ± 6.18*	68.64 ± 6.19	72.79 ± 6.77*	77.74 ± 6.95*	76.28 ± 7.16*	76.46 ± 6.89*	79.97 ± 7.18
CEs $N = 30$	81.94 ± 4.14	80.88 ± 4.23	82.59 ± 4.47	83.59 ± 4.99	81.59 ± 5.14	80.46 ± 4.86	82.54 ± 4.54
***P* value**	<0.001	0.052	<0.001	<0.001	<0.001	0.002	0.052

* $P < 0.05$.

Data are expressed in micron, reported as mean ± standard deviation; thickness values are reported for the specific analyzed areas: mean, sectors: superotemporal (ST), superior (S), superonasal (SN), inferonasal (IN), inferior (I), and inferotemporal (IT). Statistical analysis between the two groups is also reported. The mean GCL thickness is significantly lower in the FEs as compared to CEs; the subfields analysis shows a significant thinning of CGL in all sectors except temporal ones.

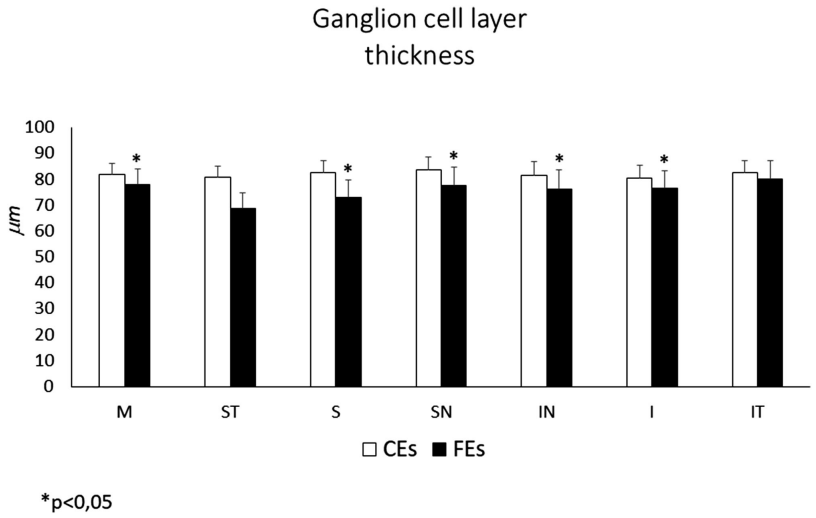

Figure 4. Histograms showing mean ganglion cell layer (GCL) thickness (expressed in micron) in FEs and CEs. GCL thickness according to the elliptical 2.4 × 2.0 mm annulus area are divided in 6 radial sectors: superior (S); superonasal (SN); inferonasal (IN); inferior (I); inferotemporal (IT); and superotemporal (ST; see Fig. 2B). The mean GCL thickness (M) in FEs is significantly reduced as compared to CEs. Subfield analysis shows in FEs a significant thinning in all sectors (S, SN, IN, and I), except for the temporal ones (ST and IT). Data are presented as mean ± SD, FEs $n = 39$, and CEs $n = 30$. 1-way ANOVA, *$P < 0.05$.

ring = 0.237 ± 0.072 vs. 0.255 ± 0.251, $P = 0.337$; outer ring = 0.209 ± 0.069 vs. 0.236 ± 0.060, $P = 0.159$; see Table 4, Fig. 5).

A deeper analysis of vitreo-retinal interface with the SS-OCT showed the presence of small focal areas of hyperreflectivity, mainly located proximally to the superficial retinal vessels in 19 of 25 (76%) FEs.

Discussion

In the present study, we analyzed and quantified the thickness of GCL by SD-OCT and analyzed the VD in the SCP and DCP in the fellow eyes of patients with unilateral IERM versus a healthy age-matched control group by SS-OCT-A. We detected a statistically significant mean reduction of GCL

Table 4. Percentage Vessel Density (VD) in the Superficial (SCP) and Deep (DCP) Capillary Plexus in 6 × 6 mm Scan of the Fellow (FEs) and Control (CEs) Eyes

	SCP			DCP		
FEs vs. CEs $N = 25$	**6 mm Mean**	**Outer Ring**	**Inner Ring**	**6 mm Mean**	**Outer Ring**	**Inner Ring**
SCP (FEs)	0.377 ± 0.076*	0.388 ± 0.068*	0.364 ± 0.102*	0.210 ± 0.065	0.209 ± 0.069	0.237 ± 0.072
SCP (CEs)	0.426 ± 0.048	0.434 ± 0.043	0.418 ± 0.064	0.233 ± 0.055	0.236 ± 0.060	0.255 ± 0.251
***P* value**	0.009	0.007	0.173	S0.173	0.159	0.337

* $P < 0.05$.

Data are reported as mean ± standard deviation. Percentage vessel density (VD) in the superficial (SCP) and deep (DCP) capillary plexus in 6 × 6 mm scan of the fellow (FEs) and control (CEs) eyes. Statistical analysis between the two groups is also reported.

The 6 mm mean VD in SCP of FEs is significantly lower than in CEs; the subfields analysis shows a significant reduction of VD in FEs also in the other sectors (inner ring and outer ring).

The 6 mm mean VD in DCP of FEs is reduced but not significantly as compared to CEs; the subfields analysis also shows a reduction, but not significant in the other sectors (inner ring, outer ring).

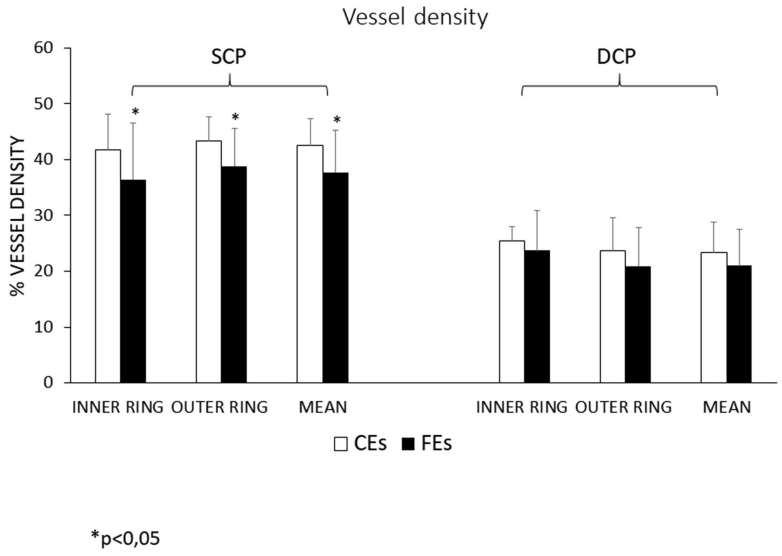

Figure 5. Histograms showing vessel density (VD) according to the 6 mm ETDRS sectors in superficial capillary plexus (SCP) (**A**) and deep capillary plexus (DCP) (**B**) in FEs and CEs. Data are shown as percentage VD. **A** VD is significantly reduced in FEs as compared to CEs in the whole ETDRS area (Mean) and in the inner and outer ring. **B** VD is reduced in FEs, as compared to CEs, in all sectors, although not reaching a statistical significance. Data are shown as mean ± SD, FEs $n = 25$, and CEs $n = 30$. 1-way ANOVA, $^*P < 0.05$.

thickness and a mean reduction of VD, although statistical significance was only found in the SCP in FEs as compared to CEs.

As previously described, the algorithm used by the Cirrus OCT to calculate the GCL measures the thickness of the tissue located between the NFL and the IPL. GCL contains astrocytes, ganglion cells, portions of Mu¨ller cells body, and blood vessels of SCP. Astrocytes distribution has been studied in anti-GFAP stained whole-mount human retina preparations; they are mainly located in the NFL and GCL, in the same regions of capillary blood vessels.[26] Astrocytes have a chamber honeycomb structure surrounding the capillaries in the retinal GCL and, therefore, they are absent in the avascular zone. With aging, the chambers become larger because of the loss of astrocytes from the vessel walls and from the astroglial bundles subdividing the astroglial chambers. This reduction in the number of astrocytes in the GCL increases progressively over time. Furthermore, the astrocytes in older people exhibit a more reactive phenotype than in younger people, with higher density of intermediate filaments but reduced total cell volume in an attempt to protect the ganglion cells from ischemia.[9] A mechanism similar to that observed in retinal ischemia in AMD could lead to the loss of astrocytes in aging, causing the death of the ganglion cells as a consequence of the reduced protection given by the astrocytes from oxidative damage. This hypothesis is supported by the finding of the significant reduction of VD in SCP of FEs (see Table 4, Fig. 5), the capillary plexus located in the GCL[19] (see Fig. 1). The loss of astrocytes could play a key role in the thinning of the parafoveal sectors observed in our study, determining consequently the ganglion cells reduction, the other principal cell-type represented in this layer.

A mean macular thickening was observed in FEs compared to CEs with variations among the different sectors. A possible pathogenic explanation of the retinal thickening may be related to the remodeling of the whole retina triggered by the damage occurring in the inner retina, elicited by the degenerative process in GCL. The observed thickening is more significant in the central (C) and parafoveal temporal inner ring (T3) sector (see Fig. 2C), although it is not significant in the other parafoveal sectors (S3, I3, and N3). These differences could be related to the distribution of the ganglion cell bodies, which in healthy eyes are normally fewer in the temporal than in the other sectors. Indeed, we found the thinning of GCL in FEs only in the S, SN, N, IN, and I sectors (see Fig. 2D). By overlapping the GCL and the whole retina thickness maps (see Fig. 2E), consequently, it can be hypothesized that the thickening of the macula is limited only to the central and temporal sectors because the S, SN, N, IN, and I sectors are thinner in the GCL.

Previous studies showed the presence of idiopathic glial projections onto the vitreal side of the ILM in aged human retinas[27,28] and that glial projections are frequently present in aged retinas and AMD.[8] Preretinal glial structures are glial projections of mainly Müller cells but also of astrocytes, which were observed in all areas of the retina, but that are most prominent near vascular areas where the ILM is most attenuated. This observation suggests that with aging, these cells normally extend their processes into the vitreous when encountering areas of ILM attenuation by forming early and mainly subclinical preretinal structures.

A previous personal study has observed an association between ERM formation and AMD (Coppe AM et al., IOVS 2011; 52: ARVO E-Abstract 3687). The more frequent presence of ERM in patients affected by diabetes, vascular diseases, or glaucoma,[1–4] in which inflammation and oxidative stress have been implicated in the pathogenesis of the ERM development led us to hypothesize that a similar, subclinical, and slowly progressive, pathogenic mechanism could also be involved in the activation of Mu¨ller cells occurring in eyes affected by IERM. Indeed, a process of retinal remodeling could be elicited by a cellular loss in the inner retina and a misguided attempt at repairing a slowly progressive ischemic/oxidative damage occurring in a preclinical stage of IERM formation. These data are also supported by the reduced VD in FEs detected in this and in a previous study[29] where a significant VD reduction of both

the SCP and DCP was found. The apparent discrepancy in the DCP, that in this study is reduced but not significantly in FEs, may be explained by the more sensitive OCT angiography utilized in this study (swept source versus spectral domain), which uses an infrared-based source and is more accurate in the analysis of the deepest retinal layers. Nevertheless, the selective alteration of the SCP is consistent with the reduction of the ganglion cells, located in the same retinal layer. The reduction of VD could be related to a loss of astrocytes, being the cause or the consequence of this event. After a primary cellular insult resulting in cellular dysfunction, as previously personally reported (2019), death of cell types located in the parafoveal inner retina in the S, SN, IN, and I sector, occurs through bystander effects or loss of trophic support. A protracted remodeling and reorganization of the remaining inner retina can subsequently lead to the migration of Mu¨ller cells along the ILM, thus, predisposing the formation of an IERM. The high percentage (76%) of focal areas of hyper-reflectivity on the vitreoretinal interface in the FEs supports the hypothesis that an epiretinal proliferation is associated with an inner retinal defect without altering the normal macular morphology in early stages of the pathogenesis.

A limitation of the study is represented by the small series of patients. Regarding other potential limitations, it has been reported that the segmentation of GCL,[30] SCP, and DCP[31] in patients with macular disorders varies among the current OCT instruments and could not be accurate; however, the outcome of our study, a reduction of GCL thickness and macular VD in SCP affecting FEs compared to CEs, is not influenced by segmentation errors as there is no spatial distortion of the subretinal layers. Moreover, FEs can be considered structurally analogous to CEs, as no anatomic modifications were present; therefore, possible segmentation errors and artifacts in SD-OCT and SS-OCT-A are identical in both groups and the comparison is not biased by them. Finally, it is well known that the presence of projection artifacts can bias the evaluation of the VD in the DCP, an intrinsic problem of the OCT-A technique; in the SS-OCT Plex 9000 used in this study a new software significantly reduced the interference of SCP in the evaluation of DCP.

In conclusion, this study documented that the FEs of patients with unilateral IERM have a significant decrease of the parafoveal ganglion cell layer associated with a decrease of VD, significant at level of the superficial capillary plexus. These findings, extending the evidence of our previous paper,[29] suggest that a primary alteration in the inner retina, due to a progressive ischemic/oxidative damage caused by decreased VD, is present in both eyes (affected and fellow eye) of patients with unilateral idiopathic ERM. This condition might precede and influence the formation of microbreaks occurring at the time of posterior vitreous detachment in the ILM that allow the migration of glial cells, astrocytes, fibroblasts, and the proliferation of an IERM. A better knowledge of the mechanism, which causes the primary cellular loss at the level of the inner retina that may determine the cascade events leading to the IERM proliferation, could permit a diagnosis of the disease in preclinical phase and provide a treatment strategy to prevent its formation.

Acknowledgments

Disclosure: **A.M. Coppe,** None; **G. Lapucci,** None; **G. Ripandelli,** None; **F.R. Pesci,** None; **L. Buzzonetti,** None; **G. Iarossi,** None

References

1. Pournaras CJ, Donati G, Brazitikos PD, et al. Macular epiretinal membranes. *Semin Ophthalmol*. 2000;15(2):100–107.
2. McCarty DJ, Mukesh BN, Chikani V, et al. Prevalence and associations of epiretinal membranes in the visual impairment project. *Am J Ophthalmol*. 2005;140(2):288–294.
3. Fraser-Bell S, Ying-Lai M, Klein R, Varma R, Los Angeles Latino Eye Study. Prevalence and associations of epiretinal membranes in Latinos: the Los Angeles Latino Eye Study. *Invest Ophthalmol Vis Sci*. 2004;45(6):1732–1736.
4. Folk JC, Adelman RA, Flaxel CJ, et al. Idiopathic Epiretinal Membrane and Vitreomacular Traction Preferred Practice Pattern Guidelines. *Ophthalmology*. 2016;123(1):P152–P181.
5. Hirokawa H, Jalkh AE, Takahashi M, et al. Role of the vitreous in idiopathic preretinal macular fibrosis. *Am J Ophthalmol*. 1986;101(2):166–169.
6. Harada C, Mitamura Y, Harada T. The role of cytokines and trophic factors in epiretinal membranes: involvement of signal transduction in glial cells. *Prog Retin Eye Res*. 2006;25(2):149–164.
7. Bringmann A, Wiedemann P. Involvement of Müller glial cells in epiretinal membrane formation. *Graefes Arch Clin Exp Ophthalmol*. 2009;247(7):865–883.
8. Edwards MM, McLeod DS, Bhutto IA, et al. Idiopathic preretinal glia in aging and age-related macular degeneration. *Exp Eye Res*. 2016;150:44–61.
9. Ramírez JM, Ramírez AI, Salazar JJ, et al. Changes of astrocytes in retinal ageing and age-related macular degeneration. *Exp Eye Res*. 2001;73(5):601–615.
10. Ridet JL, Malhotra SK, Privat A, Gage FH. Reactive astrocytes: cellular and molecular cues to biological function. *Trends Neurosci*. 1997;20(12):570–577.
11. Zhang Z, Dong F, Zhao C, et al. Natural course of vitreomacular traction syndrome observed by spectral-domain optical coherence tomography. *Can J Ophthalmol*. 2015;50(2):172–179.
12. Nesper PL, Roberts PK, Onishi AC, et al. Quantifying Microvascular Abnormalities With Increasing Severity of Diabetic Retinopathy Using Optical Coherence Tomography Angiography. *Invest Ophthalmol Vis Sci*. 2017;58(6):BIO307–BIO315.
13. Coscas F, Glacet-Bernard A, Miere A, et al. Optical Coherence Tomography Angiography in Retinal Vein Occlusion: Evaluation of Superficial and Deep Capillary Plexa. *Am J Ophthalmol*. 2016;161:160–171.e1-2.
14. Wakabayashi T, Sato T, Hara-Ueno C, et al. Retinal Microvasculature and Visual Acuity in Eyes With Branch Retinal Vein Occlusion: Imaging Analysis by Optical Coherence Tomography Angiography. *Invest Ophthalmol Vis Sci*. 2017;58(4):2087–2094.
15. Minvielle W, Caillaux V, Cohen SY, et al. Macular Microangiopathy in Sickle Cell Disease Using Optical Coherence Tomography Angiography. *Am J Ophthalmol*. 2016;164:137–144.e1.
16. Christenbury JG, Klufas MA, Sauer TC, Sarraf D. OCT Angiography of Paracentral Acute Middle Maculopathy Associated With Central Retinal Artery Occlusion and Deep Capillary Ischemia. *Ophthalmic Surg Lasers Imaging Retina*. 2015;46(5):579–581.
17. Pichi F, Sarraf D, Arepalli S, et al. The application of optical coherence tomography angiography in uveitis and inflammatory eye diseases. *Prog Retin Eye Res*. 2017;59:178–201.
18. Nagiel A, Sadda SR, Sarraf D. A Promising Future for Optical Coherence Tomography Angiography. *JAMA Ophthalmol*. 2015;133(6):629–630.
19. Campbell JP, Zhang M, Hwang TS, et al. Detailed Vascular Anatomy of the Human Retina by Projection-Resolved

Optical Coherence Tomography Angiography. *Sci Rep*. 2017;7:42201.

20. Grading diabetic retinopathy from stereoscopic color fundus photographs–an extension of the modified Airlie House classification. ETDRS report number 10. Early Treatment Diabetic Retinopathy Study Research Group. *Ophthalmology*. 1991;98(5 Suppl):786–806.
21. Mwanza JC, Durbin MK, Budenz DL, et al. Cirrus OCT Normative Database Study Group Profile and predictors of normal ganglion cell-inner plexiform layer thickness measured with frequency-domain optical coherence tomography. *Invest Ophthalmol Vis Sci*. 2011;52:7872–7879.
22. Wang RK, An L, Saunders S, Wilson DJ. Optical microangiography provides depth-resolved images of directional ocular blood perfusion in posterior eye segment. *J Biomed Opt*. 2010;15(2):020502.
23. Wang RK. Optical Microangiography: A Label Free 3D Imaging Technology to Visualize and Quantify Blood Circulations within Tissue Beds in vivo. *IEEE J Sel Top Quantum Electron*. 2010;16(3):545–554.
24. Wang RK, An L, Francis P, Wilson DJ. Depth-resolved imaging of capillary networks in retina and choroid using ultrahigh sensitive optical microangiography. *Opt Lett*. 2010;35(9):1467–1469.
25. Yousefi S, Zhi Z, Wang RK. Eigendecomposition-based clutter filtering technique for optical micro-angiography. *IEEE Trans Biomed Eng*. 2011;58(8):2316–2323.
26. Ramirez JM, Triviño A, Ramirez AI, et al. Immunohistochemical study of human retinal astroglia. *Vision Res*. 1994;34(15):1935–1946.
27. Foos RY. Posterior vitreous detachment. *Trans Am Acad Ophthalmol Otolaryngol*. 1972;76(2):480–497.
28. Foos RY. Vitreoretinal juncture; topographical variations. *Invest Ophthalmol*. 1972;11(10):801–808.
29. Coppe AM, Lapucci G, Gilardi M, et al. Alterations of macular blood flow in superficial and deep capillary plexuses in the fellow and affected eyes of patients with unilateral idiopathic epiretinal membrane. *Retina*. 2020;40(8):1540–1548.
30. Ishareef RA, Goud A, Mikhail M, et al. Segmentation errors in macular ganglion cell analysis as determined by optical coherence tomography in eyes with macular pathology. *Int J Retina Vitreous*. 2017;3:25.
31. Spaide RF, Curcio CA. Evaluation of Segmentation of the Superficial and Deep Vascular Layers of the Retina by Optical Coherence Tomography Angiography Instruments in Normal Eyes. *JAMA Ophthalmol*. 2017;135(3):259–262.

Investigative Ophthalmology & Visual Science